Physica Medica 66 (2019) 8–14

Contents lists available at ScienceDirect

Physica Medica

journal homepage: www.elsevier.com/locate/ejmp

Original paper

Evaluation of silicon based microdosimetry for Boron Neutron Capture Therapy Quality Assurance

James Vohradsky, Susanna Guatelli*, Jeremy A. Davis, Linh T. Tran, Anatoly B. Rosenfeld

Centre for Medical Radiation Physics, University of Wollongong, Wollongong, Australia

ARTICLE INFO

Keywords:
BNCT
Silicon
Microdosimetry
Geant4

ABSTRACT

The shift from reactor to accelerator based neutron production has created a renewed interested in Boron Neutron Capture Therapy (BNCT). BNCT is reliant upon the favourable uptake of ^{10}B by tumour cells along with the interaction with neutrons to produce high LET fragments (He and Li nuclei) that deposit energy locally within the tumour cells. As with any radiation based treatment, Quality Assurance (QA) is crucial. In particular, Geant4 was used to model and optimise the geometry and packaging of Silicon on Insulator (SOI) microdosimeters for BNCT Quality Assurance purposes in view of experimental measurements at the KUR research reactor, in Japan. In this context, design optimisation pertains to the sensitive volume size and probability of neutron activation. This study has shown conclusively that whilst the materials currently used in the fabrication of silicon based microdosimeters are appropriate, there are changes with respect to the sensitive volume thickness that should be addressed to reduce the number of 'stoppers' in the microdosimeter.

1. Introduction

Boron Neutron Capture Therapy (BNCT) is a type of radiotherapy that involves thermal energy neutrons, which interact with a boron distribution within the body to treat cancer. The capture of thermal neutrons by ^{10}B nuclei results in the following nuclear fission process:

$$^{10}B + n \rightarrow {}^{11}B \rightarrow {}^{7}Li + {}^{4}He + \gamma, \quad Q = 2.314\ \text{MeV} \quad 94\%$$
$$\rightarrow {}^{7}Li + {}^{4}He, \quad Q = 2.796 MeV \quad 6\%$$

The alpha particle and lithium ion produced in this reaction are high LET particles with ranges of 4.1 and 7.7 μm in tissue, respectively. In addition, protons are produced as recoil products from interactions of neutrons with ^{1}H nuclei and by ^{14}N neutron capture. Gamma rays are also produced through ^{1}H thermal capture.

Monte Carlo-based simulations have been demonstrated as a useful investigation tool for BNCT, with many facilities adopting Monte Carlo based software tools for use in BNCT Treatment Planning Systems [1–3].

The study of the effect of mixed radiation fields, such as the one of BNCT, at the cellular level can be achieved using microdosimetry [4]. Regional microdosimetry is based on the measurement of energy deposited in micron sized sensitive volumes (SV) with similar dimensions to biological cells. The lineal energy deposition is defined as follows:

$$y = \frac{E}{\langle l \rangle} \tag{1}$$

where E is the energy deposited in a SV by a traversing particle. $\langle l \rangle$ is the mean chord length calculated by means of the Cauchy formula in isotropic radiation fields:

$$\langle l \rangle = \frac{4V}{S}, \tag{2}$$

which is valid for most convex volumes in terms of its surface area (S) and total volume (V). The lineal energy (y) is a stochastic quantity. The probability distribution of lineal energy, $f(y)$, is a fundamental function in microdosimetry.

If $D(y)$ is the fraction of an absorbed dose associated with a lineal energy equal to or less than y, $d(y)$ is the dose probability density and can be determined by:

$$d(y) = \frac{dD(y)}{dy} \tag{3}$$

The dose-weighted mean lineal energy $\bar{y}_D$ is given by:

$$\bar{y}_D = \int y d(y)\, dy \tag{4}$$

$yd(y)$ vs log(y) is usually plotted in order to display the spectrum of lineal energies in greater detail.

Although currently considered the best available microdosimeter,

* Corresponding author.
E-mail address: susanna@uow.edu.au (S. Guatelli).

https://doi.org/10.1016/j.ejmp.2019.09.072
Received 31 January 2019; Received in revised form 2 September 2019; Accepted 6 September 2019
Available online 18 September 2019

the tissue equivalent proportional counter (TEPC) has several shortcomings. These limitations include: wall effects, relatively large physical size, phase effects due to measurement in gaseous phase and high operating voltage [4]. Solid state microdosimeters were proposed by the Centre for Medical Radiation Physics (CMRP), University of Wollongong (UOW) as a new method for microdosimetric measurements [5]. The concept of silicon microdosimetry aims to address the above shortcomings of the TEPC [6,7].

The microdosimetric approach studied in this work applies solid state SOI technology, which has been developed for the last twenty years at CMRP. Bradley, Rosenfeld et al. developed the first generation silicon microdosimeter, which lead to the development of dedicated microdosimeters for BNCT [4,8,9]. These devices suffered diffusion effects causing cross-talk due to ill-defined SVs. As of 2019, four generations of SOI microdosimeters have been developed by CMRP [10]. Advances in the design and fabrication of silicon microdosimeters [4,8,11,12]along with recent successes [13,14]are testimony to the feasibility of solid state microdosimetry. The research performed in this project was conducted using the latest generation V2 silicon Bridge microdosimeter design [13].

2. Method

A Geant4 simulation was developed to characterise the detector response of SOI microdosimeters in a BNCT radiation field in order to optimise their design. The probability of neutron activation was studied to investigate any potential radioprotection hazards.

Geant4 version 10.01 [15,16]was used to model the BNCT radiation field produced by an incident epithermal neutron source in a water phantom. Root v5.34 was adopted as analysis tool [17]. The simulation was based on the experimental setup adopted in Onizuka et al. (2003) at the Kyoto University Research Reactor (KUR) [18,19]. The phantom consisted of a $30 \times 30 \times 15\ cm^3$ water box and is surrounded by air. The materials used in the simulations were obtained from the *G4NistManager*, which provides material definitions derived from the NIST data reference [20].

The Geant4 Low Energy Physics Package, based on Livermore data libraries [21], was selected to describe all the electromagnetic interactions of particles, down to the recommended limit of validity of this physics model (250 eV). A default cut value of 0.01 μm was set due to the short path length of secondary particles associated with BNCT. The High Precision (HP) data libraries were adopted to describe neutron interactions at energies below 20 MeV. The HP package uses evaluated neutron data, named G4NDL4.4 which is largely sourced from the ENDF/B-VII.0 libraries [22]. The HP thermal neutron physics model was activated, as outlined in [23], to describe elastic scatter interactions in 293.15 K water and polyethylene below 4 eV. The radioactive decay was modelled as well, provided by the RadioactiveDecay 4.2 data package, which is derived from the ENSDF database [24]. Its use was crucial to investigate the neutron activation of the microdosimeter device components.

Geometrical scaling factors can be used in solid-state microdosimetry to convert energy deposition in silicon to a tissue equivalent response. For BNCT microdosimetry, a suitable scaling factor of approximately 0.63 has been determined [9], which has been applied to all results presented in this study. The 1.47 MeV alpha particle produced in BNCT has a range of 5 μm and 8 μm in silicon and tissue, respectively.

The modelled incident radiation field consisted of a 5 cm diameter cylindrical beam of epithermal neutrons which originate on one side of the water phantom. The neutron energy fluence was based on the KUR reactor operating in epithermal mode, as shown in Fig. 1.

The first simulation was designed to calculate the optimal depth in the water phantom to place the detector to maximize BNCT reactions. For this simulation, 25 parts-per-million ^{10}B was distributed uniformly in the water, which is the typical concentration of ^{10}B in the tumour for BNCT. The optimal depth is located at the depth of 27 mm in the water phantom to maximise the number of recorded BNCT reactions. Section 3.1 shows the results deriving from this study. The detector probe used by CMRP, which houses the Bridge microdosimeter, was modelled and positioned at the optimal depth within the water phantom, facing the incident beam direction as shown in Fig. 2.

A PMMA layer with thickness equal to 500 μm in the direction of incidence of the neutron beam, 100 μm thick polyethylene (PE), the boron conversion layer with varying thickness, the 100 μm air gap and Bridge microdosimeter follow. The PMMA layer represents the waterproof outer casing which houses the detector components. The removable neutron converter in the setup consists of a 3 μm thin film of enriched boron carbide ($^{10}B_4C$) deposited on a 170 μm aluminium substrate. PE tape is used to attach the converter layer onto the top of the detector package. This leaves a thin air gap between the microdosimeter and the converter film. The Bridge microdosimeter is shown from bird's eye view in Fig. 3.

The second simulation focused on the optimisation of detector geometry for the CMRP SOI Bridge microdosimeter in terms of its SV geometry. Microdosimetry is only appropriate in radiation environments where the particles incident on the detector have a range that exceeds the mean chord length of the SV [25]. That is, most events within the SVs must pass through the device (crossers). Those which have shorter range than the mean chord length range and come to rest within the SV are undesired (stoppers). Therefore it is essential to increase the relative number of crossers versus stoppers interacting with the SVs. This work investigates the proportion of stoppers and crossers in the microdosimetric spectra with respect to three key variables: SV thickness, SV lateral area and thickness of the $^{10}B_4C$ converter film. Reduction in the SV thickness and SV area will reduce the mean chord length of the SVs, which should increase the number of crossers. Unfortunately, a compromise has to be reached as smaller SV sizes, which favour crossers against stoppers, reduce the sensitivity of the detector and may require a larger array of SVs, translating into an overall bigger device.

The use of boron conversion films which have a thickness close to the range of the products originated in it is problematic. This is because the BNCT products lose more energy within the converter leading to a higher probability of stoppers in the SV. As a means of verifying the most optimal experimental set-up, the $^{10}B_4C$ film thickness is investigated with respect to the ratio of crossers/stoppers within the target SV. Another site of BNC reactions is the built-in boron doped p+ region of the SVs [9]. It is expected that particles produced in this region will have greater range than those in the converter film, allowing for more crossers in the SVs. The relative number of BNC particles reaching the SVs and type of interaction will be compared for the $^{10}B_4C$ film and p+ region of the SVs.

The secondary radiation field produced in the microdosimeter by the incident BNCT neutron field was studied as well. This mainly relates to the radioprotection of experiment operators and the investigation of background noise that could be produced in the detector. The flux of the KUR epithermal neutron beam was used to calculate the relative number of incident particles required in the simulation for a 5 cm diameter cylindrical beam. The detector was simulated to be irradiated for the typical BNCT treatment time of 30 min. In the simulation, the track history of each particle was recorded, such as information regarding the parent particle and which physics process produced it. For each interaction, the kinetic energy, the point where the secondary particle is generated and its final location, when it comes to rest, is also stored. The rate at which materials produced dangerous levels of ionising radiation and the required cool-down of the detector time was investigated. This was achieved by modelling the rate of neutron activation during irradiation and the time required for radioactivity to fall below 1 μBq. This lower activity threshold was chosen as it is well below the limit of concern given by the IAEA for the materials tested [26].

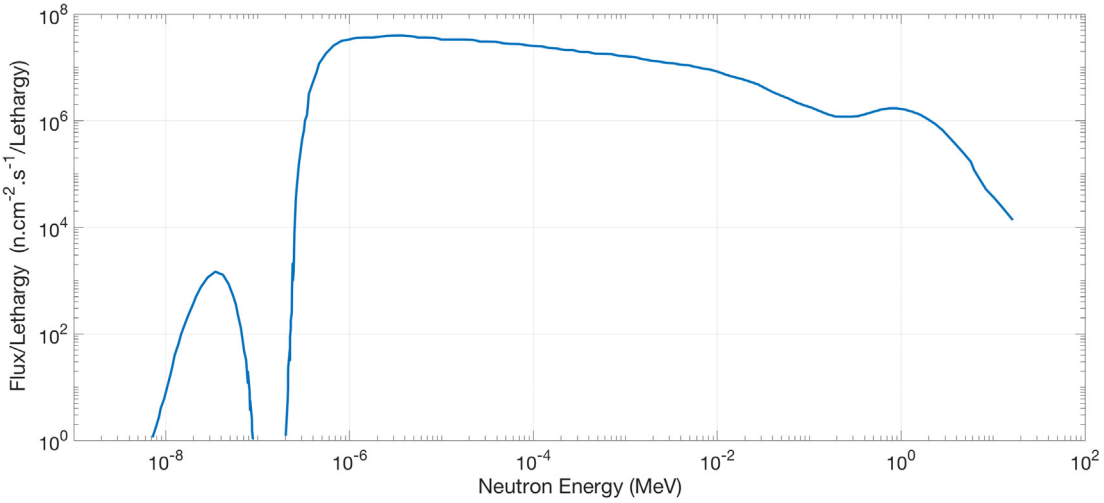

Fig. 1. KUR epithermal neutron energy spectrum used as the primary source in all simulations [18], courtesy of Baba et al.

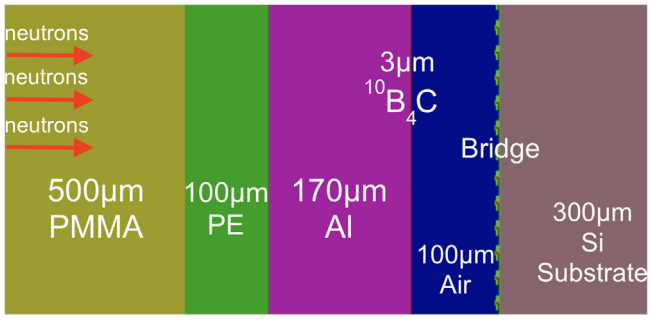

Fig. 2. Detail of the geometry of the detector and its packaging, in the direction of incidence of the neutron beam (incident from left). The neutron beam has a diameter exceeding the lateral sizes of the microdosimeter device. The microdosimeter is set at 2.7 cm depth in the water phantom.

3. Results

3.1. Depth dose calculation in water

The simulated depth-dose response is depicted in Fig. 4. The maximum response for alpha particles, lithium nuclei and protons was 22, 23 and 31 mm, respectively. Using this result, the optimal depth was chosen to be 27 mm. This placement is consistent with experimental measurements obtained by Onizuka et al. (2003) [19].

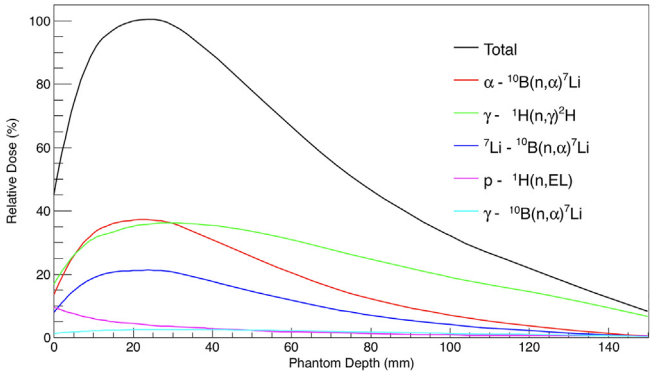

Fig. 4. Depth dose curve in the water phantom, with 25 ppm ^{10}B uniformly distributed in water. The total energy deposition is depicted in black. The contribution deriving from each secondary particle under investigation is indicated as well, together with the process originating the secondary particle (see the legend).

3.2. Geometry optimisation of the SVs of the SOI bridge microdosimeter for BNCT quality assurance

3.2.1. Sensitive volume thickness reduction

In order to increase the number of crossers in the microdosimeter, the thickness of the SVs was reduced in the direction of incidence to the neutron beam. Three different thicknesses were considered in this study: 10, 2 and 1 µm, with their microdosimetric responses shown in Figs. 5–7, respectively.

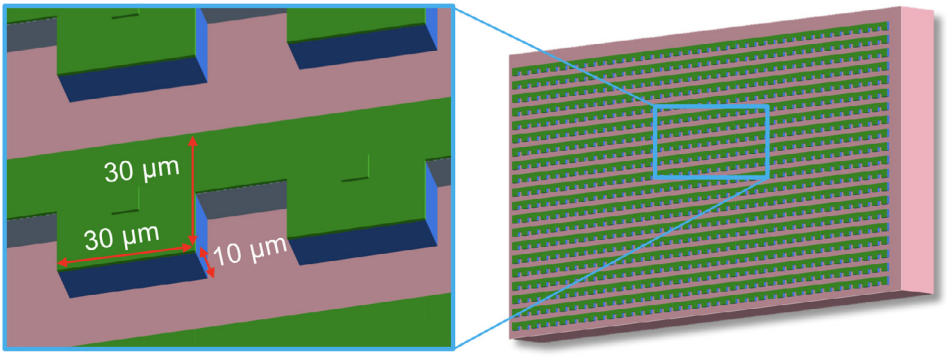

Fig. 3. Bridge SOI Microdosimeter. The SVs shown in green have dimensions of $30 \times 30\,\mu m^2$ with 10 µm thickness along the direction of incidence of the neutron beam.

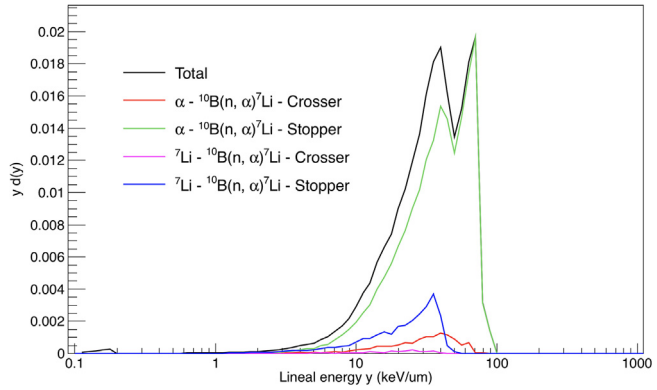

Fig. 5. Microdosimetric spectra of $30\times30\times10\,\mu m^3$ SOI Bridge SVs with $3\,\mu m$ thick $^{10}B_4C$ film (mostly stoppers).

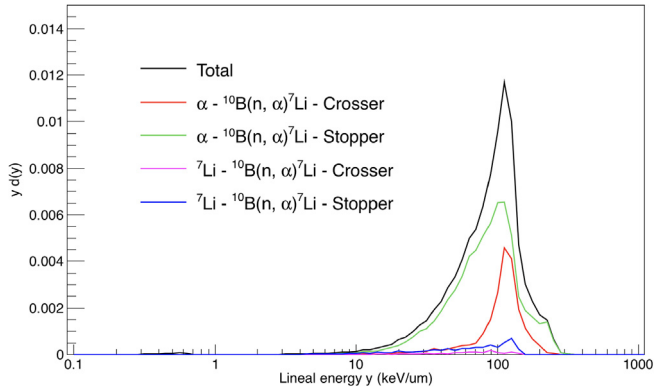

Fig. 6. Microdosimetric spectra of $30\times30\times2\,\mu m^3$ SOI Bridge SVs with $3\,\mu m$ thick $^{10}B_4C$ film (increased crossers).

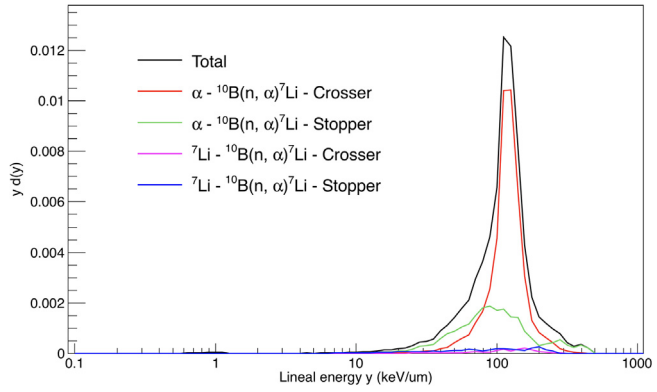

Fig. 7. Microdosimetric spectra of $30\times30\times1\,\mu m^3$ SOI Bridge SVs with $3\,\mu m$ thick $^{10}B_4C$ film (mostly crossers).

The range of the 1.47 MeV alpha particles and 0.84 MeV ^{7}Li nuclei produced by BNC in silicon are 5.26 μm and 2.46 μm, respectively [27]. A-priori knowledge of the range of these particles provides a means of optimising the detector geometry. It is obvious that the current SOI microdosimeter would be unsuitable for BNCT given the thickness (10 μm) is greater than the maximum range of the BNCT products.

Table 1 shows the proportion of crossers and stoppers by particle compared with the total for different SV thicknesses. The current Bridge design with 10 μm thick SVs yielded a response which mostly consisted of stoppers. With the SV thickness design reduced to 2 μm, as shown in Fig. 6, the fraction of crossers is about 40%, which is approximately 7.6 times higher. For the conceptual design which uses 1 μm thick SVs, as shown in Fig. 7, the number of crossers were further increased.

Table 1
Ratio of crosser or stopper by particle type to total for different detector designs and 3 μm thick B_4C.

Detector Design	B_4C	Crossers		Stoppers	
		α	^{7}Li	α	^{7}Li
$30\times30\times10\,\mu m^3$ SV	3 μm	0.043	0.003	0.827	0.070
$30\times30\times2\,\mu m^3$ SV	3 μm	0.253	0.009	0.640	0.042
$30\times30\times1\,\mu m^3$ SV	3 μm	0.616	0.020	0.272	0.035

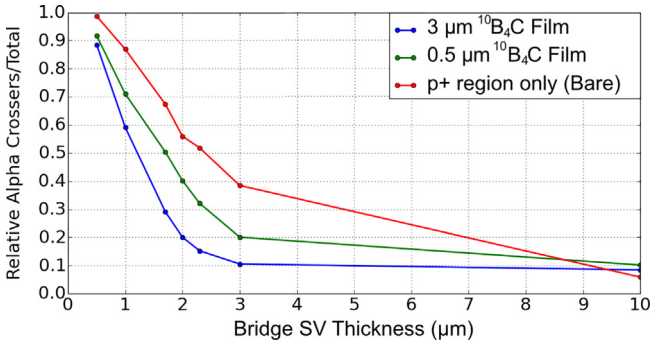

Fig. 8. Relative ratio of alpha particle crossers and total number of alpha particle crossers and stoppers in the microdosimeter SVs obtained using the 3 μm B_4C thick film (blue) and 0.5 μm B_4C thick film (green). The ratio of crossers/total in the bare detector is obtained using only the boron doped p+ region implanted in the SVs is depicted in red. (For interpretation of the references to colour in this figure legend, the reader is referred to the web version of this article.)

However, due to limitations with the current technology used for detector fabrication, only the 2 μm thick SV design is feasible.

3.2.2. *Reduced boron carbide film thickness*

The current design of the boron converter is based upon what will be used experimentally. Fig. 8 shows the fraction of alpha particles crossing the SV, for two different $^{10}B_4C$ thicknesses (3 μm, 0.5 μm) and for bare detector with doped p+ region.

For the 3 μm thick $^{10}B_4C$ film, the alpha particles and ^{7}Li nuclei emerging from the film had an overall lower kinetic energy due to ionisation. As such, larger angles of incidence are prevented, which shaped the field to increase propagation in one direction towards the SVs. The range of the 1.47 MeV alpha particle produced by BNC in $^{10}B_4C$ is approximately 3.43 μm [17].

The proportion of alpha particles and ^{7}Li nuclei in terms of crosser and stoppers are shown in Table 2 for the 0.5 μm thick $^{10}B_4C$ layer. The count collected by the device with $30\times30\times2\,\mu m^3$ SVs compared with that of $30\times30\times10\,\mu m^3$ SVs is 105 counts/s and 78 counts/s, respectively, which is approximately 26% less. This should be taken into consideration, as an increase in the number of SV in the array may be required. Unlike the results shown in Table 1 with the 3 μm thick $^{10}B_4C$ film, the relative number of alpha and ^{7}Li particles are much closer in

Table 2
Ratio of crosser or stopper by particle type to total for different detector designs and 0.5 μm thick B_4C.

Detector Design	B_4C	Crossers		Stoppers	
		α	^{7}Li	α	^{7}Li
$30\times30\times10\,\mu m^3$ SV	0.5 μm	0.102	0.038	0.426	0.434
$30\times30\times2\,\mu m^3$ SV	0.5 μm	0.400	0.143	0.125	0.332
$10\times10\times2\,\mu m^3$ SV	0.5 μm	0.497	0.370	0.026	0.106
$10\times10\times1\,\mu m^3$ SV	0.5 μm	0.508	0.432	0.009	0.051

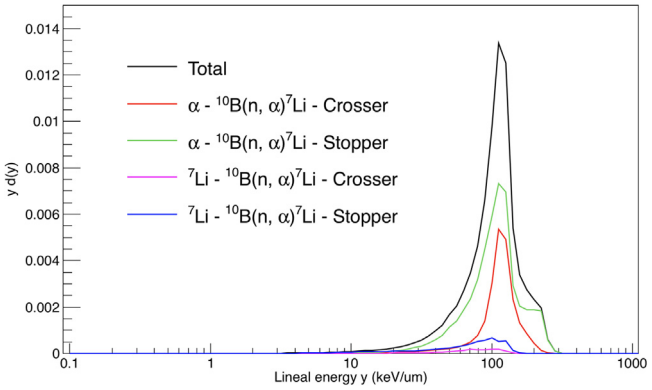

Fig. 9. Microdosimetric spectra of $30\times30\times2\,\mu m^3$ SOI Bridge SVs with 0.5 μm thick $^{10}B_4C$ conversion film.

value for the $30\times30\times10\,\mu m^3$ SV device.

For the 0.5 μm thick $^{10}B_4C$ layer, the distribution of the radiation field that emerges from the film is more isotropic with higher kinetic energy. This provides an advantage of more crossers in the SVs. The number of alpha particles and ^{7}Li nuclei that reach the SVs is twice as much. The microdosimetric spectra obtained with $30\times30\times2\,\mu m^3$ SVs using this film thickness is shown in Fig. 9. The lower energy alpha stoppers have been minimised with this configuration, but a shoulder between 120 and 250 keV/μm is now present due to larger angles of incidence of emission from the film.

Another site of BNC reactions is the boron doped p+ region of the SVs. For the alpha particles produced in this built-in neutron converter, the rate of crossers are much higher than the $^{10}B_4C$ film. This was due to a lower energy loss of alpha particles as they did not have to pass through overlayers to reach the SV. This result validated the feasibility of applying the boron doped p+ region in SOI microdosimeters for dedicated BNCT microdosimetry. However, the rate of ^{10}B(n, α)^{7}Li reactions in the p+ region is approximately 500 times lower than the $^{10}B_4C$ film. The detection rate of these products from the p+ region by the SVs is 9.6 counts/s.

3.2.3. Sensitive volume lateral width reduction

The changes to the microdosimetric spectra relative to the lateral area of the device is presented in Fig. 10. The lateral area was reduced from $30\times30\,\mu m^2$ to $10\times10\,\mu m^2$. The decreasing volume size should lead to lower mean chord lengths and higher probability of crossers. However, as the lateral area is smaller, interactions with the SV by normally incident particles is lower. As such, the proportion of stoppers in this case are mostly high energy alpha particles, which enter the SV at extreme angles.

Table 2 also describes the ratio of interaction types between alpha particles and ^{7}Li nuclei in terms of the lateral width of the SVs. The equivalent mean chord length of SVs with smaller lateral area allow for a much higher probability of crossers. However, the total count of these smaller SVs is significantly reduced. The count rate for the $10\times10\times2\,\mu m^3$ and $10\times10\times1\,\mu m^3$ SVs is 8.1 counts/s and 7.6 counts/s, respectively. Compared with the $30\times30\times10\,\mu m^3$ SV device, the count rate is approximately 92% lower.

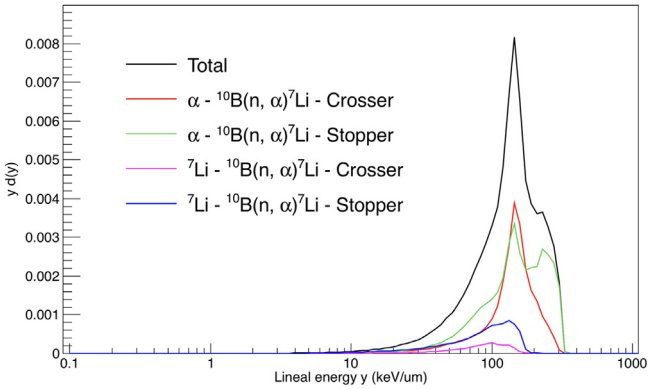

Fig. 10. Microdosimetric spectra of $10\times10\times2\,\mu m^3$ SOI Bridge SVs with 0.5 μm $^{10}B_4C$ conversion film.

Provided the current technology using a detector with 2 μm thick SVs, the worst case scenario would require the number of counts deriving from the BNCT reactions to be higher than 1000, to be well above the noise threshold. This poses a potential issue when using thinner SVs and only using products from the p+ region. The theoretical designs using 0.5 μm film plus $30\times30\times2\,\mu m^3$, $10\times10\times2\,\mu m^3$ and p+ region only would need to be exposed for 15, 123 and 104 s, respectively, to have sufficient counts. Given the typical treatment time of 30 min for BNCT, this should not cause major concern.

3.3. Activation and fragmentation in experimental setup

The reaction rate that occurred in the SOI Bridge and detector probe materials during neutron irradiation by the KUR epithermal source is shown in Table 3. The detector configuration consists of $30\times30\times2\,\mu m^3$ SVs and a 0.5 μm thick B_4C film. Figs. 11 and 12 show the radiation field and activity curve of secondary particles produced in the detector materials, respectively. For the SOI Bridge microdosimeter, most activations are associated with silicon and aluminium, which have high nuclear cross sections in this neutron energy range. Interactions in silicon occur mainly in the substrate of the microdosimeter.

There are minimal recoils in the same energy range as BNCT products. Scattered protons arising from neutron moderation have kinetic energy mainly lower than 1.5 MeV. The significant production of deuteron by ^{1}H thermal capture had very low kinetic energy and range of only a few micron in water [27], so it does not pose a particular concern.

In terms of radioprotection, ^{28}Al and ^{31}Si have a high activation rate. Following the beam shut-off, ^{28}Al takes less than 2 h to reach 1μBq. For ^{31}Si, it would take over 376 years of constant irradiation to reach the

Table 3
Interactions within the SOI Bridge microdosimeter and detector probe materials (see Fig. 2) resulting from neutron irradiation.

Reaction	Count/s	Material
^{10}B(n, α)^{7}Li	5.35×10^{3}	$^{10}B_4C$ Film (99.82%), p+ region (0.18%)
^{1}H(n,G)^{2}H	3.19×10^{2}	PMMA (77.96%), PE (22.04%)
^{28}Si(n,G)^{29}Si	5.96×10^{1}	Si Substrate (99.57%), SV (0.63%), SiO_2 (0.2%)
^{27}Al(n,G)^{28}Al	5.91×10^{1}	Al Film (100%)
^{12}C(n,G)^{13}C	3.51×10^{0}	PMMA (82.37%), PE (17.63%)
^{29}Si(n,G)^{30}Si	1.90×10^{0}	Si Substrate (98.31%), SV (1.13%), SiO_2 (0.56%)
^{30}Si(n,G)^{31}Si	1.58×10^{0}	Si Substrate (99.32%), SiO_2 (0.68%)
^{10}B(n,G)^{11}B	5.33×10^{-1}	$^{10}B_4C$ Film (100%)
^{28}Al→^{28}Si Decay	3.05×10^{-1}	Al Film (96.61%), Si Substrate (3.39%)
^{14}N(n,p)^{14}C	2.35×10^{-1}	Air Gap (100%)
^{18}O(n, α)^{15}C	9.60×10^{-2}	PMMA (100%)
^{13}C(n,G)^{14}C	7.46×10^{-2}	PMMA (85.71%), PE (14.29%)
^{10}B(n,2α + t)	3.20×10^{-2}	$^{10}B_4C$ Film (100%)
^{28}Si(n, α)^{25}Mg	3.20×10^{-2}	Si Substrate (100%)
^{15}C→^{15}N Decay	2.72×10^{-2}	PMMA (100%)
^{16}O(n, α)^{13}C	2.13×10^{-2}	PMMA (100%)
^{14}N(n,G)^{15}N	2.13×10^{-2}	Air Gap (100%)
^{29}Si(n, α)^{26}Mg	1.07×10^{-2}	Si Substrate (100%)
^{28}Si(n,p)^{28}Al	1.07×10^{-2}	Si Substrate (100%)
^{18}O(n,G)^{19}O	1.07×10^{-2}	PMMA (100%)
^{19}O→^{19}F Decay	2.74×10^{-4}	PMMA (100%)
^{31}Si→^{31}P Decay	1.16×10^{-4}	Si Substrate (99.32%), SiO_2 (0.68%)

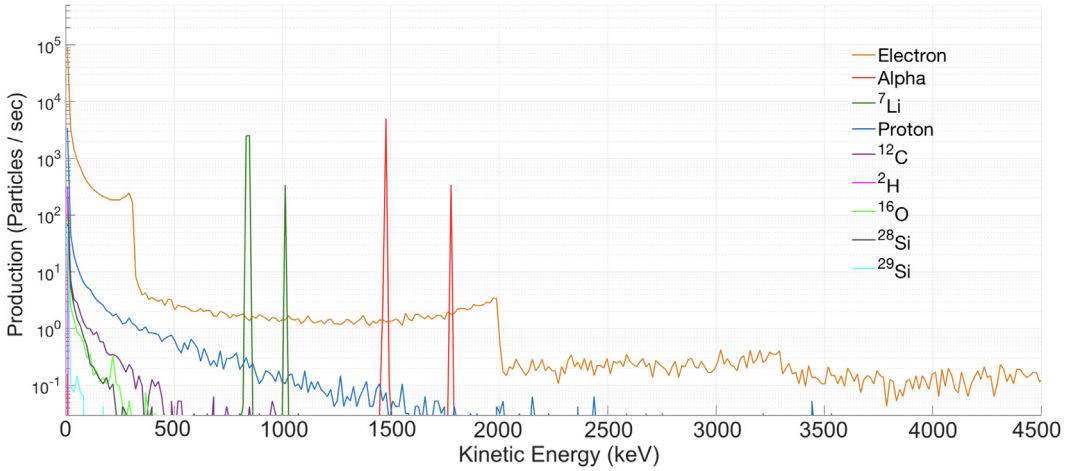

Fig. 11. Secondary radiation field produced by the KUR epithermal neutron field in the materials of the SOI microdosimeter device.

IAEA activity limit of 10^6Bq [26]. It is important to note that all activations of ^{28}Al occurred in the aluminium film of the neutron converter, with a negligible count in the aluminium tracks of the detector.

The gamma ray spectrum produced in the detector materials is shown in Fig. 13. The major gamma ray energy peak at 478 keV is due to BNC reactions, which occurs with 94% of the captures. Due to the high abundance of hydrogenous materials, the thermal capture of ^{1}H with prompt gamma emission is observed at 2.23 MeV. Prompt gamma lines associated with ^{27}Al captures occur with a high rate due to its high nuclear cross section. Aluminium may pose a potential concern if larger quantities are used, such as the addition of a frame for the water phantom, due to its high activation rate. However, it is not an issue for the current design, with only a few hours of cooldown required following a 30 min irradiation period.

4. Discussion and conclusions

This study has shown conclusively that whilst the materials currently used in the fabrication of SOI microdosimeters are appropriate in terms of radioprotection, there are changes with respect to the sensitive volume size that should be addressed for the application of SOI microdosimetry to BNCT. The 3D Bridge microdosimeter with 2 μm SV thickness and $30 \times 30\,\mu m^2$ SV lateral area is the most feasible design for BNCT QA using the current fabrication technology. SVs with thickness of 1 μm or less have been shown to be more suitable for microdosimetry but are currently unable to be manufactured. However, the reduction in sensitivity must be taken into account when considering smaller SVs. Compared with the 10 μm thick SV, the total reduction in counts for the 2 μm and 1 μm SVs are approximately 26% and 30% less, respectively.

Thinner $^{10}B_4C$ films are required to decrease the energy loss of BNC products, in order to enhance the number of SV crossers. This also has the advantage of shaping the field emerging from the film to be more isotropic. The boron implanted p+ region in the SVs provided an adequate source of BNC products, which were mostly crossers. However, it has a much lower count rate than the $^{10}B_4C$.

The activation study has shown that the device does not pose any significant concern in terms of radiation protection for use in epithermal mode BNCT. However, the production of secondary nuclear recoils can contribute to the background noise in the detector, which must be taken into account. Alternative substrates for the neutron conversion film will be investigated in future work.

Future work will involve the modelling of the electrical and charge collection characteristics of the ideal SOI microdosimeter in Synopsys TCAD for BNCT applications. These results will be compared with experimental measurements. This study supports the characterisation of the response of the SOI Bridge microdosimeter, for when it will be irradiated at the KUR reactor.

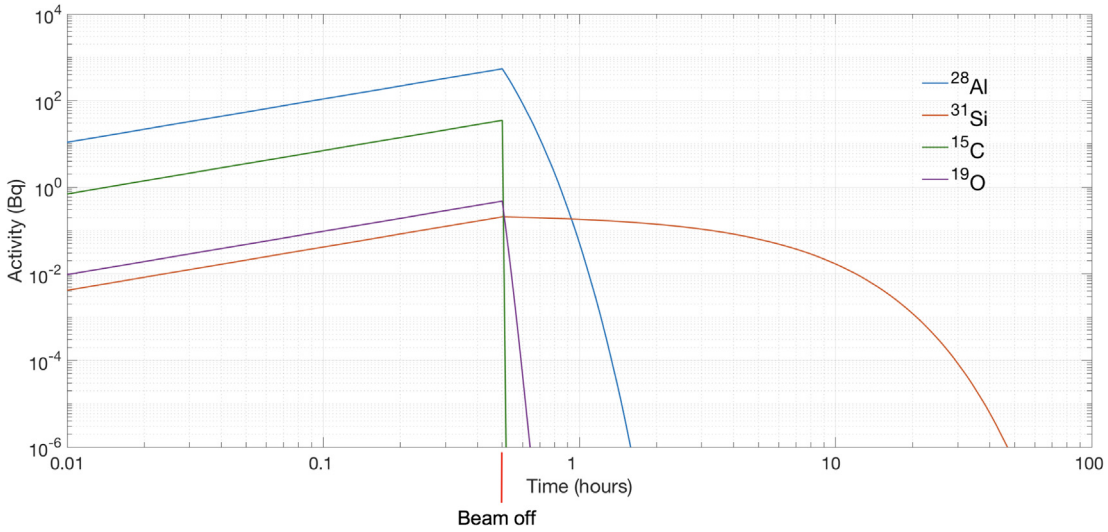

Fig. 12. Activity of radioisotopes produced within the materials of the SOI Bridge detector device for 30 min irradiation period with cool-down.

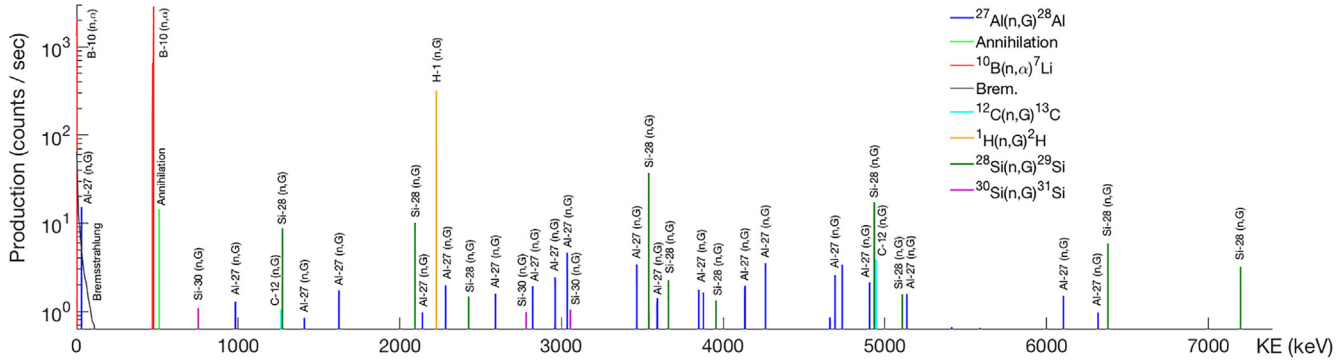

Fig. 13. Gamma ray spectrum produced in SOI detector probe materials by the KUR epithermal neutron source.

Acknowledgements

This research was supported through the Australian Government Research Training Program (RTP) and CMRP faculty office scholarships. The authors would like to thank UOW Information Management and Technology Services (IMTS) for computing time on the UOW High Performance Computing Cluster.

References

[1] Nigg D, Wemple C, Wessol DE, Wheeler FJ, Albright C, Cohen M, Frandsen M, Harkin G, Rossmeier M. SERA – an advanced treatment planning system for neutron therapy and BNCT. Trans Am Nucl Soc 1999;80.

[2] Kumada H, Matsumura A, Sakurai H, Sakae T, Yoshioka M, Kobayashi H, Matsumoto H, Kiyanagi Y, Shibata T, Nakashima H. Project for the development of the linac based NCT facility in University of Tsukuba. Appl Rad Isotopes 2014;88:211–5. https://doi.org/10.1016/j.apradiso.2014.02.018.

[3] Lin TY, Liu YWH. Development and verification of THORplan – a BNCT treatment planning system for THOR. Appl Rad Isotopes 2011;69:1878–81. https://doi.org/10.1016/j.apradiso.2011.03.025.

[4] Bradley PD, Rosenfeld AB, Allen B, Coderre J, Capala J. Performance of silicon microdosimetry detectors in boron neutron capture therapy. Rad Res 1999;151:235–43. https://doi.org/10.2307/3579934.

[5] Rosenfeld AB, Kron T, D'Errico F, Moscovitch M. Advanced semiconductor dosimetry in radiation therapy. AIP Conf Proc 2011;1345:48–74. https://doi.org/10.1063/1.3576159.

[6] Bradley PD, Rosenfeld AB, Zaider M. Solid state microdosimetry. Nucl Instrum Methods Phys Res Sect B 2001;184:135–57. https://doi.org/10.1016/S0168-583X(01)00715-7.

[7] Bradley PD, Rosenfeld A, Lee KK, Jamieson D, Heiser G, Satoh S. Charge collection and radiation hardness of a SOI microdosimeter for medical and space applications. IEEE Trans Nucl Sci 1999;45:2700–10.

[8] Bradley PD. The development of a novel silicon microdosimeter for high LET radiation therapy [Ph.D. thesis]. Australia: University of Wollongong; 2000.

[9] Bradley PD, Rosenfeld AB. Tissue equivalence correction for silicon microdosimetry detectors in boron neutron capture therapy. Med Phys 1998;25:2220–5. https://doi.org/10.1118/1.598421.

[10] Rosenfeld AB. Novel detectors for silicon based microdosimetry, their concepts and applications. Nucl Instrum Methods Phys Res Sect A 2016;809:156–70. https://doi.org/10.1016/j.nima.2015.08.059.

[11] Cornelius I, Rosenfeld AB, Siegele R, Cohen DD. Improvement of SOI microdosimeter performance using pulse-shape discrimination techniques. IEEE Trans Nucl Sci 2002;49:2805–9. https://doi.org/10.1109/TNS.2002.805411.

[12] Ziebell AL, Lim WH, Reinhard MI, Cornelius I, Prokopovich DA, Siegele R, Dzurak AS, Rosenfeld AB. A cylindrical silicon-on-insulator microdosimeter: charge collection characteristics. IEEE Trans Nucl Sci 2008;55:3414–20. https://doi.org/10.1109/TNS.2008.2004464.

[13] Tran LT, Chartier L, Bolst D, Prokopovich DA, Guatelli S, Nancarrow M, Reinhard MI, Petasecca M, Lerch MLF, Pereverlaylo VL, Matsufuji N, Hinde D, Dasgupta M, Stuchbery A, Jackson M, Rosenfeld AB. 3D silicon microdosimetry and RBE study using 12C ion of different energies. IEEE Trans Nucl Sci 2015;62:3027–33. https://doi.org/10.1088/1742-6596/777/1/012037.

[14] Tran LT, Guatelli S, Prokopovich DA, Petasecca M, Lerch MLF, Reinhard MI, Ziegler JF, Zaider M, Rosenfeld AB. A novel silicon microdosimeter using 3D sensitive volumes: modeling the response in neutron fields typical of aviation. IEEE Trans Nucl Sci 2014;61:1552–7. https://doi.org/10.1109/TNS.2014.2298461.

[15] Agostinelli S, Allison J, Amako K, Apostolakis J, Araujo H, Arce P, Asai M, Axen D, Banerjee S, Barrand G. GEANT4 – a simulation toolkit. Nucl Instrum Methods Phys Res Sect A 2003;506:250–303. https://doi.org/10.1016/S0168-9002(03)01368-8.

[16] Allison J, Amako K, Apostolakis J, Araujo H, Dubois P. Geant4 developments and applications. IEEE Trans Nucl Sci 2006;53:270–8. https://doi.org/10.1109/TNS.2006.869826.

[17] Brun R, Rademakers F. ROOT – an object oriented data analysis framework. Nucl Instrum Methods Phys Res Sect A 1997;389:81–6. https://doi.org/10.1016/S0168-9002(97)00048-X.

[18] Baba H, Onizuka Y, Nakao M, Fukahori M, Sato T, Sakurai Y, Tanaka H, Endo S. Microdosimetric evaluation of the neutron field for BNCT at Kyoto University reactor by using the PHITS code. Rad Protect Dosim 2011;143:528–32. https://doi.org/10.1093/rpd/ncq511.

[19] Onizuka Y. Microdosimetry with TEPC of boron containing wall. Proceeding of the scientific meeting 2002 on advancement of the system for neutron capture therapy KURRI-KR-95. Research Reactor Institute Kyoto University; 2003. p. 53–8.

[20] Shen VK, Siderius DW, Krekelberg WP, Hatch HW. NIST standard reference simulation website – National Institute of Standards and Technology. NIST Standard Reference Database Number 173; 2017.https://doi.org/10.18434/T4M88Q.

[21] Rodrigues P, Chauvie S, Guatelli S, Ivanchenko V, Longo F, Mantero A, Mascialino B, Nieminen P. Geant4 low energy electromagnetic physics. IEEE Symp Conf Record Nucl Sci 2004. https://doi.org/10.1109/NSSMIC.2004.1462612.

[22] IAEA. Evaluated Nuclear Data File (ENDF), Version 2017-10-03. URL:https://www-nds.iaea.org/exfor/endf.htm; 2017 [accessed 1 February 2019].

[23] Garcia AR, Mendoza E. Validation of the thermal neutron physics in GEANT4. G4 Hadronic group meeting. Gobeierno de Espana: Ciemat; 2013.

[24] IAEA. ENSDF Database, Version 2015-12. URL:https://www-nds.iaea.org/relnsd/NdsEnsdf/QueryForm.html; 2015 [accessed 01.02.2019].

[25] International Commission on Radiation Units and Measurements. ICRU Report 36: Microdosimetry Technical Report; 1983.

[26] IAEA. Radiation protection and safety of radiation sources: international basic safety standards technical report; 2011.

[27] Ziegler JF, Ziegler MD, Biersack JP. SRIM the stopping and range of ions in matter. Nucl Instrum Methods Phys Res Sect B 2010;268:1818–23. https://doi.org/10.1016/j.nimb.2010.02.091.